

# A Neutral Hydrogen Survey of Polar-Ring Galaxies: I. Green Bank Observations of the Northern Sample

O.-G. Richter

*Hamburger Sternwarte, Gojenbergsweg 112, 2050 Hamburg 80, Germany*

P. D. Sackett

*Institute for Advanced Study, Princeton, NJ 08540*

L. S. Sparke

*University of Wisconsin, 475 N. Charter St, Madison, WI 53706*

## Abstract

We present the results of a neutral hydrogen survey conducted with the Green Bank 140-foot radio telescope of 47 northern objects in the polar-ring galaxy atlas of Whitmore *et al.* (1990). We detected 39 of these above our detection limit of  $1.7 \text{ Jy} \cdot \text{km s}^{-1}$ ; the average measured flux of  $21 \text{ Jy} \cdot \text{km s}^{-1}$  corresponds to an average neutral hydrogen mass of  $5.3 \times 10^9 M_{\odot}$  for a Hubble constant of  $H_0 = 75 \text{ km s}^{-1} \text{ Mpc}^{-1}$ . For the polar-ring galaxies in our sample that have also been observed with radio arrays, we find that the  $21'$  (FWHM) Green Bank beam often includes much more flux than found by the synthesis instruments for the polar rings alone; some of these galaxies are known to have gas-rich companions. We compare the neutral hydrogen content of the sample to the blue luminosity and IRAS fluxes. The HI-to-blue-light ratios of the confirmed and probable polar rings are around unity in solar units, indicating that polar ring galaxies (or their environments) are as gas-rich as typical irregular galaxies. For their blue luminosity, the confirmed polar rings are underluminous in the far-infrared, as compared with the rest of the sample. They are also FIR-underluminous for their HI masses, which suggests that most of the gas in the ring may be in stable orbits, rather than flowing inward to trigger star formation in the central galaxy. The more disordered class of 'related objects,' which includes a number of obvious mergers, is highly luminous in the far-infrared.

Submitted to *The Astronomical Journal*.

# 1 Introduction

A polar-ring system consists of a flattened galaxy with an outer ring of gas, dust, and stars rotating in a plane approximately orthogonal to the central galaxy. The central object is an elliptical or S0 galaxy and thus generally devoid of gas and dust. Polar rings probably represent merger products, and their study may give us valuable clues about the process and frequency of merging (Schweizer *et al.*, 1983, hereafter SWR). In addition, measurements of rotation in the two nearly-perpendicular planes of the ring and galaxy provide one of the few probes of the three-dimensional shape of galactic gravitational potentials, and hence the shape of the dark matter halos (SWR, Whitmore *et al.*, 1987, hereafter WMS, and Sackett & Sparke, 1990, hereafter SS). Until recently, only about 20 polar-ring candidates were listed in the literature (SWR); but a new photometric atlas of polar-ring galaxies (Whitmore *et al.*, 1990; hereafter PRC) now substantially increases the number of known polar-ring galaxies and candidates to over 100.

All but one of the few polar-ring galaxies that have been mapped in the 21cm line of neutral hydrogen contain substantial gas, often a few billion solar masses (assuming a Hubble constant  $H_0 = 75 \text{ km s}^{-1} \text{ Mpc}^{-1}$  used throughout this paper), which is morphologically associated with the optical ring and shares similar kinematics (Shane 1980, Schechter *et al.*, 1984, and van Gorkom *et al.*, 1987). The combination of this large gas content and relatively low blue luminosities give polar-ring galaxies gas-to-light ratios  $M_{\text{HI}}/L_{\text{B}}$  near unity (Sackett 1991), even larger than those characteristic of spiral galaxies (Giovanelli & Haynes 1988).

We undertook the Green Bank 140-foot neutral hydrogen survey described here primarily to identify a larger sample of polar-ring systems rich enough in HI to be suitable for subsequent high-resolution mapping in the 21cm line. Such mapping measures the distribution and the velocity field of gas in the rings, both of which are required for an accurate determination of the shape of the dark matter halo in these systems (*cf.*, SS). Together with optical absorption-line studies of the central galaxies, rotation in the ring gas can determine whether morphological candidates are true kinematical polar rings. Furthermore, knowledge of the ring mass is necessary in order to assess the stability of the ring against differential precession, an important consideration in dating the ring and hence, presumably, measuring the time since its formation. Sparke (1986) has shown that self-gravitating polar rings can remain stable in a slightly non-polar configuration with a gentle warping toward the pole, but only if the total ring mass exceeds a lower limit set by the gravitational potential of the central galaxy. Since the neutral hydrogen mass in polar rings may constitute a substantial fraction of the total ring mass, measuring the HI content of a larger sample of polar rings should show whether self-gravity is generally important in these systems. Additionally, our Green Bank data provide the first measure of the redshift of two galaxies in our sample.

## 2 The Polar-Ring Galaxy Sample

The objects in the PRC are divided into four main categories:

- A: Kinematically-confirmed polar-ring galaxies (6 objects)
- B: Good candidates for polar-ring galaxies (27 objects)
- C: Possible candidates for polar-ring galaxies (73 objects)
- D: Systems possibly related to polar-ring galaxies (51 objects)

The search procedure used to generate the catalog of these relatively rare objects was neither systematic nor complete, and the typing of objects into the four main categories listed above was necessarily subjective. The identification of polar rings is hampered by the fact that their appearance is strongly affected by ring brightness and viewing angle. Nevertheless, the PRC provides the current best compilation of galaxies with an optical component that is severely inclined to the plane of the central object.

Our initial source list consisted of all objects in the PRC with declinations north of  $-45^\circ$  satisfying one or more of the following criteria: (1) known redshift, or (2) measured blue magnitude  $m_B$  brighter than 15.5, or (3) member of PRC category A or B (see above). Of the resulting 99 objects, 70 had known redshifts, and 15 had no measured redshifts but were brighter than  $m_B = 15.5$ . The remaining 14 objects were members of PRC category B with unknown redshifts.

We then checked the electronically-available HI catalog of Huchtmeier and Richter (1989) for previously measured fluxes and eliminated several well-observed galaxies from our source list, although we did reobserve some of these galaxies in order to compare fluxes within the relatively large beam of the Green Bank 140-foot telescope with those from other telescopes with smaller beams. Finally, we discarded all galaxies with known redshifts above  $8000 \text{ km s}^{-1}$ . (One target was later found to be listed as slightly fainter than  $m_B = 15.5$  in newer catalogs, and, prior to the observing run, one B category galaxy was measured to have a redshift in excess  $8000 \text{ km s}^{-1}$ ; we retained both galaxies in our sample.) The resulting source list consisted of 58 objects, 11 of which we were unable to observe because of strong interference from the Sun, leaving a working sample of 47 objects.

With the Parkes 64m telescope, we have also carried out similar observations of polar-ring objects with declinations below the southern limits of Green Bank; those results will be reported in a subsequent paper. Observations of many of the detected galaxies in our northern sample and others that we were unable to observe due to interference have been made with the Effelsberg 100m radio telescope (Huchtmeier *et al.*, in preparation).

### 3 The HI Observations and Results

The data were obtained during a 9-day observing run in August and September of 1990 at the NRAO<sup>1</sup> 140-foot radio telescope (GB 140') in Green Bank, WV. The receiver was the one used previously at the former 300-foot telescope. The system noise temperature varied with elevation: at best it was 18K; at worst it was about 30K for targets close to the southern declination limit of  $-45^\circ$ . The backend was the Mark IV autocorrelator with 1024 channels, which was split into four banks of 256 channels each with an IF bandwidth of 10 MHz. Both polarizations were fed into two autocorrelator banks set to cover the same frequency band in order to recover about 8% of the quantization loss during the autocorrelation. The velocity resolution was thus  $8 \text{ km s}^{-1}$ . Most ON-source scans were 10 minutes long; only the strongest nearby HI sources (*i.e.*, NGC 660 and all secondary HI-line calibrators) were observed for shorter periods. The ON-scans followed corresponding OFF-source scans of equal duration taken at positions generally 10.5 minutes earlier in right ascension. Where the relative positions of program galaxies were favorable, we were able to increase our efficiency by using a single OFF-source scan for more than one galaxy. At least two ON/OFF scan pairs were obtained for all galaxies. Due to strong interference from the Sun between  $9^h 30^m$  and  $11^h 30^m$ , some objects that were on our original list could not be observed, namely those galaxies with PRC designations B-9 (UGC 5119), C-30 (UGC 5101), C-32 (IC 575), C-33 (ESO 500-G41), C-37 (UGC 6182), D-08 (ESO 305-G21), D-12 (UGC 4892), D-14 (UGC 5485), D-16 (NGC 3406), D-23 (NGC 4753), and D-24 (AM 1257-222).

Figure 1 shows plots of the spectra obtained, after subtraction of a polynomial baseline fit; the fit was generally 4th order, though higher-order fits were used where the signal was strong. Antenna temperature in mK (where  $1 \text{ Jy} = 0.277\text{K}$ ) is plotted on the vertical scale in Fig. 1; sources in the OFF-beam appear as 'absorption' features in the plotted spectra. In 39 of the 47 galaxies that we observed, HI flux was detected above the  $3\text{-}\sigma$  r.m.s. noise level in at least one channel, in profiles that were reproducible in subsamples of equal duration. For those galaxies observed with the longest integration times, this corresponds to a flux detection limit of  $1.7 \text{ Jy} \cdot \text{km s}^{-1}$  for a flat-topped line with a  $250 \text{ km s}^{-1}$  linewidth, or a lower limit on the neutral hydrogen mass of about  $1 \times 10^9 M_\odot$  of HI at 50 Mpc. The average detected flux for this sample of 39 galaxies at the GB 140' was  $21 \text{ Jy} \cdot \text{km s}^{-1}$ , corresponding to an average detected HI mass of  $5.3 \times 10^9 M_\odot$ . The average linewidth of our detected galaxies is  $260 \text{ km s}^{-1}$ . Due to an unreliable optical redshift, one target, NGC 5122, was observed at an incorrect radial velocity; subsequently, it has been detected in the 21cm line at the VLA (Cox, *et al.*, 1994, in preparation).

---

<sup>1</sup>The National Radio Astronomy Observatory is operated by AUI, Inc. under a cooperative agreement with the National Science Foundation





**Fig. 1** Spectra obtained at the Green Bank 140-foot (GB 140') radio telescope. Antenna temperature is shown in mK on the vertical scale; the horizontal scale is displayed in  $\text{km s}^{-1}$  along the bottom of each spectra. Each spectrum is the result of subtracting one or more ON-source/OFF-source pairs and has been baseline-subtracted and Hanning-smoothed (except UGC 5600 and NGC 660, which have not been smoothed). See Table 1 and the Appendix for details about individual objects.

Table 1 gives the results of our HI observations and related optical data. In columns 1 and 2 we give the PRC number of the galaxy and its conventional name; columns 3 and 4 the B1950.0 coordinates; columns 5 and 6 the optically-measured heliocentric radial velocity and its bibliographic source; columns 7 and 8 the total blue magnitude  $B_T$  of each galaxy with its source; columns 9 and 10 the logarithm of the optical major axis diameter and its source; column 11 the newly-determined HI heliocentric radial velocity; columns 12 and 13 the integrated flux and its mean error; column 14 the HI linewidth at 20% of the peak; and finally, columns 15 and 16 the peak flux density and r.m.s. flux density.

For non-detections, column 11 gives the velocity range searched, and the total flux integral and peak flux density represent upper limits. The upper limit on the peak flux density in column 15 is taken to be 3 times the r.m.s. noise; this is integrated over a ‘top-hat’ profile of width  $250 \text{ km s}^{-1}$  to obtain the upper limit on the flux integral given in column 12. If the undetected systems are similar to those that we did detect, these upper limits are conservative for most objects since the HI profiles are more sharply peaked than the flat-topped box we have assumed.

Signals detected in the OFF-scan for a given galaxy are reported in the subsequent line in Table 1, and are labeled with ‘OFF.’ To properly interpret the data in Table 1 for individual galaxies, and for comments about the individual spectra, the reader is referred to the notes in the Appendix. Optical photographs of the galaxies in our sample can be found in the polar-ring atlas of Whitmore *et al.* (PRC, 1990).

A few qualifications must be made. The optical data do not form a homogeneous set; where possible we have used information from the Third Reference Catalog (de Vaucouleurs *et al.* 1991, hereafter RC3), but in general have had to draw from a variety of sources; the key to these sources is given in the caption to Table 1. If detailed optical studies have been performed on particular galaxies, we have used values from these works rather than those from the RC3. Since polar rings are often faint, the catalogued diameter measurements will sometimes refer to the size of the ring and sometimes to the size of the central host galaxy. The blue magnitudes have been collected from a variety of sources and cannot be assumed to be on the same scale. In some cases the total blue magnitude,  $B_T$  was unavailable, and the apparent blue magnitude,  $m_B$ , has been reported instead.

In Table 2 we present infrared data collected for the galaxies in our sample. Columns 1 and 2 give the PRC identification and the conventional name for the galaxy; column 3 identifies the bibliographic source of the IRAS flux densities as either the Faint Source Catalog-Version 2 (FSC2), co-added scans, or an integrated infrared map; columns 4, 5, 6, and 7 give flux densities in the 12-, 25-, 60- and 100-micron bands of IRAS, respectively; columns 8, 9, 10, and 11 the corresponding flux qualities; column 12 the logarithm of the total far-infrared flux; and columns 13, 14 and 15 the 12/25, 25/60 and 60/100 infrared colors. Only flux densities with quality 2 or better were used for the calculation of the infrared colors. For flux











densities determined from co-added scans, columns 8-11 indicate whether the source was resolved in each of corresponding IRAS bands.

All IRAS fluxes were retrieved electronically from NED<sup>2</sup>. For inclusion in NED, FSC2 sources must pass criteria that are designed to filter out most stars, including a required detection in the 60 micron band (*i.e.*, flux quality greater than one) greater than one-half the 25 micron flux. Consequently, it is possible that some identifications have been missed, and statistical statements about the 25/60 color of our sample should be avoided. The FSC2 is signal-to-noise ratio limited and, because of reliability requirements, does not achieve the full sensitivity of the Faint Source Survey (FSS) plates, but is about a factor of 2 to 2.5 times more sensitive than the Point Source Catalog (PSC). Typically, the FSS contains sources with flux densities above 0.2 Jy at 12, 25, and 60 microns, and above 1.0 Jy at 100 microns, though due to uncertain subtraction of infrared cirrus, especially at 100 $\mu$ , precise limits will vary with the location of the source on the sky.

The far-infrared flux,  $F_{\text{FIR}}$ , is taken here to be given by

$$F_{\text{FIR}} = 1.26 \times 10^{-14} (2.58 f_{60} + f_{100}) \text{ W} \cdot \text{m}^{-2} \quad (1)$$

where  $f_{60}$  is the flux density at 60 $\mu$  and  $f_{100}$  is the flux density at 100 $\mu$  in Jy. This prescription is used by IPAC (Lonsdale *et al.* 1989) to represent the total far-infrared flux that would be emitted by a thermal source with the indicated flux densities through a perfect bandpass of 80 microns centered on 82.5 $\mu$ . This representation is valid for dust temperatures between 20K and 80K and dust emissivity indices  $n$  (emissivity  $\propto \nu^{+n}$ ) from 0 to 2, which are thought to be the ranges relevant to galaxies. Color corrections have not been applied. If the flux density in one of these two bands has flux quality equal to one, and therefore represents only an upper limit, the corresponding upper limit on  $\log [F_{\text{FIR}}]$  is given in column 12. The infrared colors given in columns 13, 14, and 15 are defined here as  $\log [f_{12}/f_{25}]$ ,  $\log [f_{25}/f_{60}]$ , and  $\log [f_{60}/f_{100}]$  respectively.

Table 3 contains quantities derived from the basic optical, radio, and infrared parameters given in Tables 1 and 2. Columns 1 and 2 give the PRC number and conventional name for the galaxy; column 3 an abbreviation for the radio telescope used; column 4 the computed distance to the source; column 5 the HI mass for the indicated observation; columns 6 and 7 the blue and far-infrared luminosities; and columns 8, 9, and 10 a measure of the ratios of luminosities in the blue, far-infrared, and the 21cm line.

Distances in Table 3 are derived from radial velocities referred to the centroid of the Local Group according to the prescription of the Revised Shapley-Ames Catalog

---

<sup>2</sup> The NASA/IPAC Extragalactic Database (NED) is operated by the Jet Propulsion Laboratory, California Institute of Technology, under contract with the National Aeronautics and Space Administration.





(Sandage & Tammann 1987; RSA), namely

$$v_{\text{LG}} = v_{\text{helio}} + [ -79 \cos \ell \cos b + 296 \sin \ell \cos b - 36 \sin b ] \quad \text{km} \cdot \text{s}^{-1} \quad (2)$$

Wherever possible, the newly-determined radial velocities from this work are used to compute the distance; for non-detections, optical velocities from Table 1 are used instead. The HI mass from our Green Bank observations is calculated directly from the flux integral and the distances derived from these observations, and does *not* include any correction factors, such as for the source (over-)filling the beam. That is, we use simply

$$M_{\text{HI}} = 2.356 \times 10^5 D_{\text{Mpc}}^2 \int S_{\nu, \text{Jy}} \cdot dv_{\text{km s}^{-1}} \quad M_{\odot} \quad (3)$$

For the kinematically-confirmed polar-ring galaxies, which are given the ‘A’ classification in the PRC, we have searched the literature for other HI measurements with which to compare our fluxes. Wherever possible, the  $M_{\text{HI}}$  quoted from these works has been converted to our Hubble constant and velocity zero-point for inclusion in Table 3 and in the Appendix. If the total flux integral and heliocentric velocity have been given in the original work, we use them together with equations (1) and (2) and our Hubble constant to derive a distance and an HI mass. If the assumed distance and a heliocentric velocity are given, we compute a distance based on our assumptions as described above, and then multiply the HI mass in the original work by the square of the ratio of these two distances to give the mass in Table 3. If only an assumed Hubble constant and heliocentric velocity are given in the original work, the original HI mass is multiplied by the square of the Hubble constant ratio to obtain the HI mass appropriate to our Hubble constant. In the cases for which we detected no HI emission, an upper limit on the HI mass is calculated from the optically-measured redshift and the upper limit on the flux integral listed in Table 1.

The total blue and far-infrared luminosities are computed using the distances given in column 4, and the magnitudes and fluxes from Tables 1 and 2. The blue magnitudes are corrected for external extinction from dust in the Milky Way using the  $A_{\text{B}}$  values given in the RC3; no correction is made for extinction internal to the galaxies themselves. The resulting blue luminosity is given in column 6 of Table 3 relative to the solar blue luminosity,  $L_{\odot, \text{B}}$ , while in column 7 the far-infrared luminosity is normalized to the bolometric luminosity of the Sun,  $L_{\odot}$ ; solar quantities are taken from Appendix 1A of Binney and Tremaine (1987). For the computation of the ratio of far-infrared to blue luminosities given in column 9 of Table 3, the fluxes  $F_{\text{FIR}}$  and  $F_{\text{B}}$  were first converted to common units of  $\text{W} \cdot \text{m}^{-2}$  so that the resulting ratio is unitless.



## 4 Discussion

Our survey indicates that polar-ring galaxies are associated with much more neutral hydrogen than is usual for early-type galaxies. Figure 2 shows the HI mass as a function of distance for all 39 galaxies of our sample that were detected with the GB 140', and five upper limits for systems for which redshifts were independently available; the detection limit of  $1.7 \text{ Jy} \cdot \text{km s}^{-1}$  is shown as the dashed line. In this and all subsequent figures, Kinematically-Confirmed polar rings (PRC Category A) are shown as filled circles; Good Candidates (PRC Category B) are shown as filled squares; Possible Candidates (PRC Category C) are shown as open squares; and Related Objects (PRC Category D) are shown as open stars.

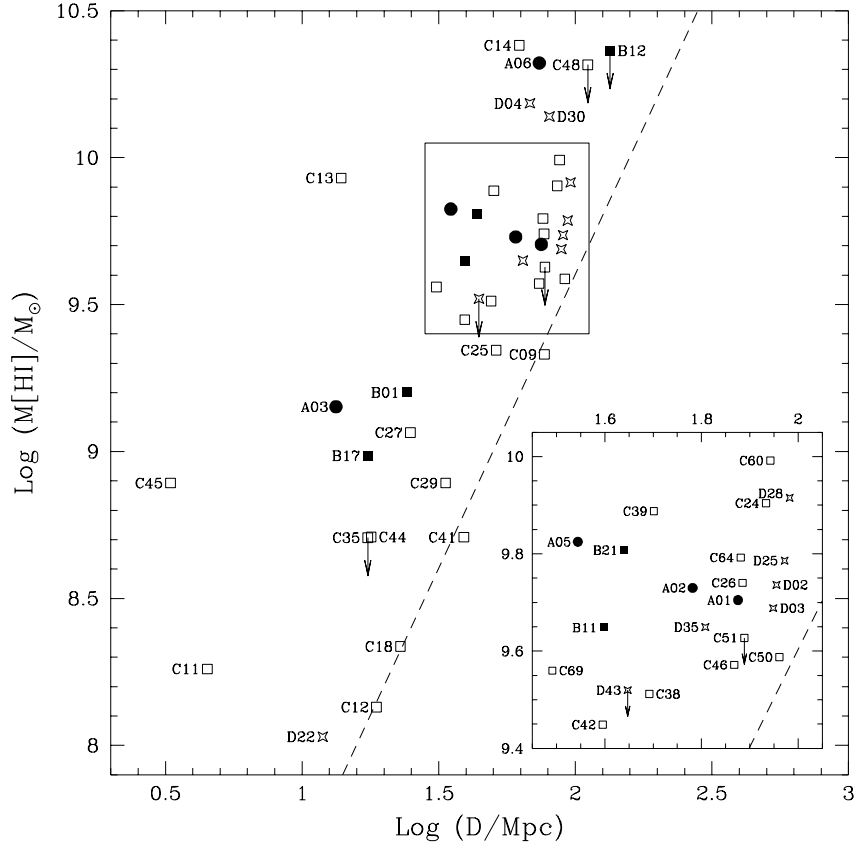


**Fig. 2** The derived HI mass (or upper limits) as a function of distance,  $D$ , for the galaxies in the GB 140' sample. Galaxies given the PRC designations A, B, C, and D, are shown as filled circles, filled squares, open squares, and open stars, respectively. The detection limit  $1.7 \text{ Jy} \cdot \text{km s}^{-1}$  of the observations is shown as the dashed line. The insert magnifies the region near  $D = 51 \text{ Mpc}$  and  $M_{\text{HI}} = 4.5 \times 10^9 M_{\odot}$ , the median values of the distance and HI mass for the detected galaxies in our sample.

The average detected gas mass for our sample is  $M_{\text{HI}} = 5.3 \times 10^9 M_{\odot}$ , about twice the level of the S0 galaxies detected in the survey of Wardle and Knapp (1986). Objects with  $M_{\text{HI}} > 6 \times 10^9 M_{\odot}$  include members of all four categories of the PRC. Based on the results of earlier synthesis mapping, we would expect that the HI in a polar-ring system is associated with the ring and not with the central galaxy; consistent with this, our HI profiles fall off steeply at the sides and have linewidths typical of galactic rotation, as they should if the gas follows stable orbits extending well into the flat portion of the rotation curve. This is in contrast to the HI profiles in small groups of galaxies, where sloping shoulders on the velocity profile are a signature of tidal interaction (Gallagher, Knapp & Faber 1981).

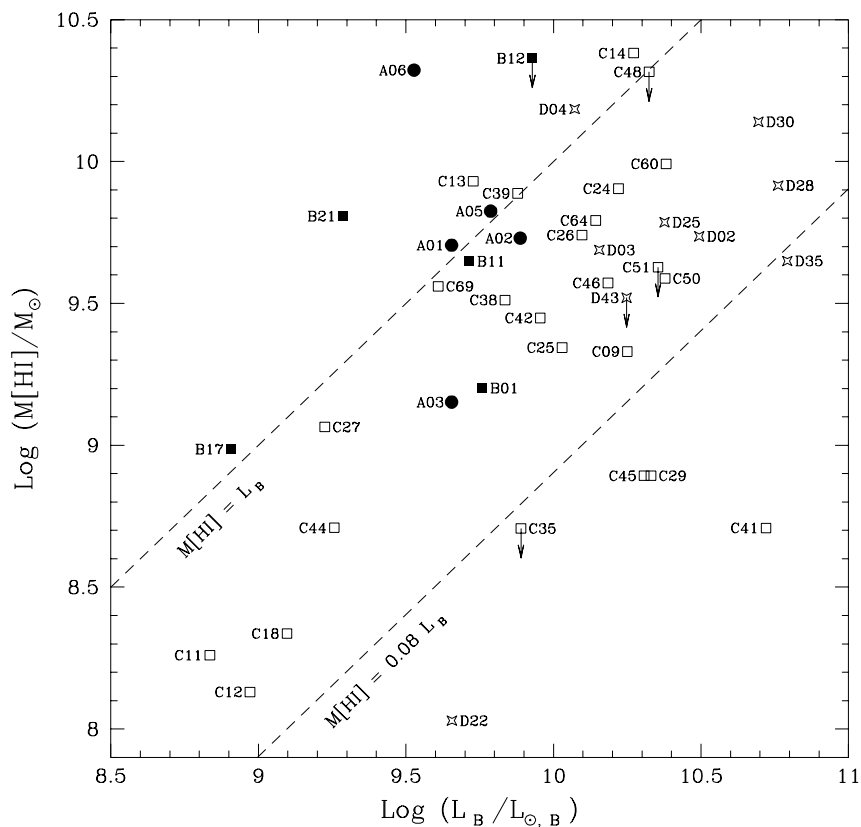


**Fig. 3** The HI mass as a function of blue luminosity for the galaxies of the GB 140' sample; solar units are used. The upper dashed line represents the typical gas-richness of irregular galaxies,  $M_{\text{HI}}/L_B = 1$ ; the lower line represents a value more typical of S0 galaxies,  $M_{\text{HI}}/L_B = 0.08$ .

The neutral hydrogen mass is shown as a function of blue luminosity in Figure 3; the upper dashed line indicates a gas-to-light ratio of  $M_{\text{HI}}/L_B = 1$  in solar units, characteristic of galaxies later than type Sc (Giovanelli & Haynes 1988), and of the most gas-rich dwarfs in Virgo (Bothun *et al.* 1985). Objects from PRC Categories A

and B cluster about this line, while most from Categories C and D lie well below it, but still above the mean of  $M_{\text{HI}}/L_{\text{B}} = 0.08$  that Wardle and Knapp (1986) derived for their S0 sample. The ‘Kinematically Confirmed’ polar rings and the ‘Good Candidates’ thus show more gas mass per unit blue light than the ‘Possible Candidates’ and ‘Related Objects.’ Gas-rich Category C and D objects are optically bright, while Categories A and B consist of rather faint galaxies, all with  $L_{\text{B}} \leq 10^{10} L_{\odot}$ , that are disproportionately gas-rich compared to the rest of the sample.

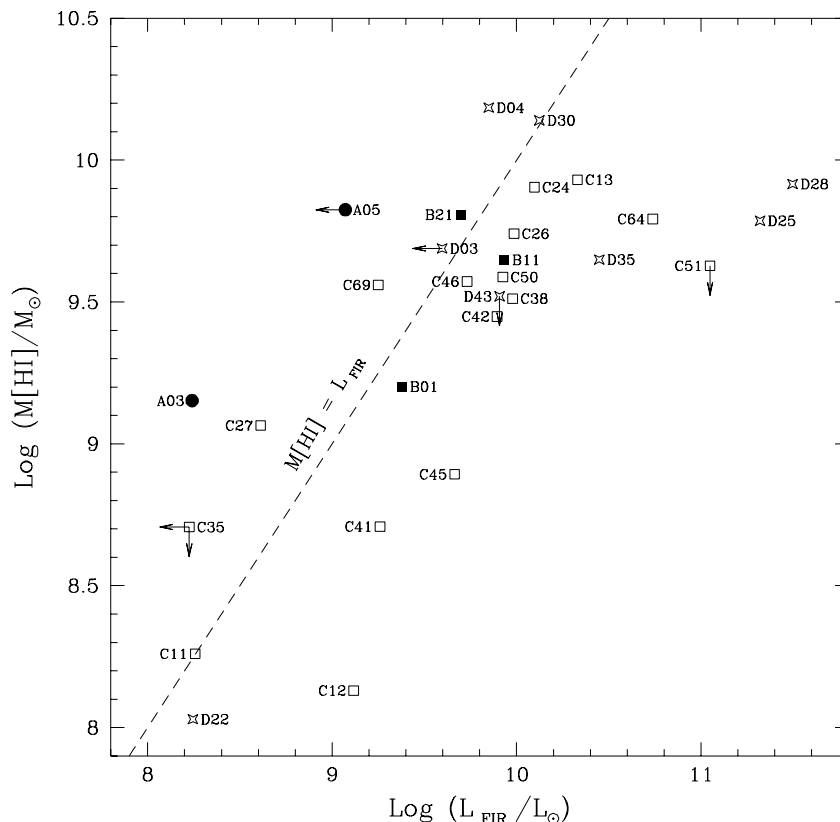


**Fig. 4** The HI mass as a function of far-infrared luminosity in solar (bolometric) units for the GB 140' sample.

Figure 4 compares the neutral hydrogen mass with the far-infrared luminosity,  $L_{\text{FIR}}$ , which measures emission from warm dust. The Category C and D systems that are most overluminous in the far-infrared for their HI mass, compared with the mean of our sample, are known interacting and merging galaxies. The two confirmed polar-ring systems (Category A objects) are the two most gas-rich galaxies in the sample for their FIR luminosity. The three other confirmed polar rings in our sample were not detected by IRAS; if we use rough upper limits for their 60 and 100 micron fluxes of 0.2 and 1 Jy respectively, we find that all three have  $M_{\text{HI}}/L_{\text{FIR}} > 1$  in solar

units. The far-infrared fluxes for the 26 galaxies of our GB 140' sample that were detected in both the 60 and 100 micron bands of IRAS vary over more than three orders of magnitude, with a median value of  $L_{\text{FIR}} = 8.0 \times 10^9 L_{\odot}$  somewhat below the median value of  $L_{\text{FIR}} = 1.3 \times 10^{10} L_{\odot}$  derived for a sample of interacting galaxies by Bushouse, Lamb & Werner (1988). The median value of  $L_{\text{FIR}}$  for the 7 Category D galaxies is about equal to the median value for the Bushouse *et al.* interacting sample, while the median of the Category A and B galaxies is about an order of magnitude lower.

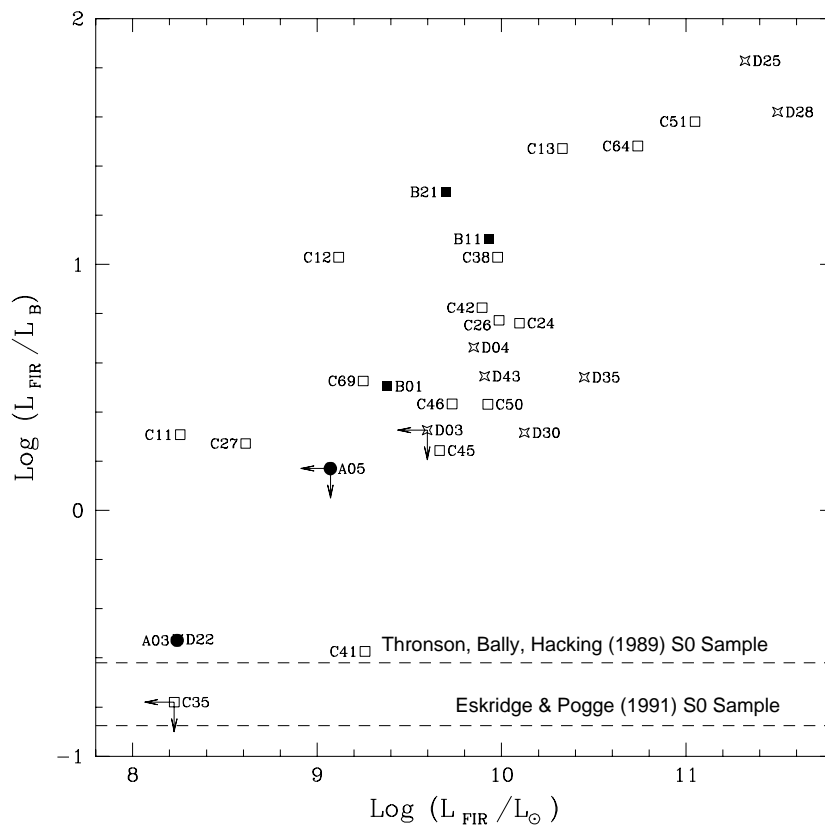


**Fig. 5** The ratio of far-infrared to blue luminosities (in  $\text{W} \cdot \text{m}^{-2}$ ) plotted as a function of blue luminosity (in solar bolometric units) for the galaxies of the GB 140' sample. For comparison, the mean values of  $\log [L_{\text{FIR}}/L_{\text{B}}]$  are shown as dashed lines for two S0 samples in the literature.

Figure 5 shows the ratio of far-infrared to blue light as a function of FIR luminosity for our sample; the luminosities have now been converted to common units of  $\text{W} \cdot \text{m}^{-2}$ . The median value of  $L_{\text{FIR}}/L_{\text{B}}$  for the complete GB 140' sample is 4.1, to be compared with 5.6 reported by Bushouse *et al.* (1988) for their interacting sample, and 3.0 for their isolated sample of galaxies. Ring galaxies, in which active star formation is seen in a ring that is coplanar with the central galaxy, are thought to be the result of

a head-on collision with a small intruder; these galaxies have a larger average far-infrared luminosity,  $L_{\text{FIR}} = 2.1 \times 10^{10} L_{\odot}$  (corrected to our  $H_0$ ), than our sample, but a considerably smaller  $L_{\text{FIR}}/L_{\text{B}} = 0.86$  (Appleton & Struck-Marcell 1987).

Even given their disturbed morphology, it is a little surprising that *all* of the galaxies in our polar-ring sample are more FIR-luminous for their blue light than the mean value of  $\log [L_{\text{FIR}}/L_{\text{B}}] = -0.875$  derived by Eskridge and Pogge (1991) for a sample of S0 galaxies. Eskridge and Pogge estimated the internal extinction in their sample when calculating  $L_{\text{B}}$ , and performed a survival analysis that took into account upper limits; both would tend to lower their mean value relative to our analysis. Thronson, Bally and Hacking (1989) estimated  $\log [(2.56f_{60} + f_{100})/f_{\text{B}}] = 1.5$  for a variety of S0 subtypes from the RSA, where  $f_{60}$ ,  $f_{100}$  and  $f_{\text{B}}$  are flux *densities*. When these are converted to fluxes this corresponds to  $\log [L_{\text{FIR}}/L_{\text{B}}] = -0.62$ , considerably below most of our sample, but consistent with Eskridge and Pogge’s result within the large uncertainties of this measurement. Non-detections by IRAS of three Category A polar rings in our sample places upper limits on their  $\log [L_{\text{FIR}}/L_{\text{B}}]$  of 0.4 to 0.9. The one confirmed polar-ring galaxy (NGC 2685) for which IRAS measured flux in both the 60 and 100 $\mu$  bands has  $L_{\text{FIR}}/L_{\text{B}}$  and a 60/100 color similar to that found for early-type galaxies; Thronson *et al.* (1989) found the same to be true for their sample of shell galaxies, where the structure is also thought to represent an ‘undigested’ merger.

Figures 4 and 5 taken together show that, compared to the rest of our sample, the two confirmed polar rings detected by IRAS are severely underluminous in  $L_{\text{FIR}}$  for their blue luminosity and their HI mass. A possible explanation is that in polar-ring systems the dust resides mainly in the rings, along with the HI, while the stars that could heat it to IRAS-emitting temperatures are mostly in the central galaxy; much of the dust in these systems may thus be too cool to emit in the IRAS wavebands. The very red 60/100 infrared color of NGC 2685, the reddest in our sample, is consistent with primary dust heating from an older population of disk stars, rather than from the UV radiation of OB stars (Bothun, Lonsdale & Rice 1989). In their study of S0 galaxies, Eskridge and Pogge (1991) find that of the objects which are atypically HI rich for their IRAS flux, many of those that have been mapped in HI have their gas in outer rings rather than in the inner disk (van Driel & van Woerden 1991); this is a similar situation to polar rings. The low FIR emission of polar-ring galaxies suggests that the gas is in stable orbits in the ring, rather than flowing rapidly in to the central galaxy, where it would lead to star formation. As illustrated by Figure 6, the objects of our sample show no obvious trend of gas-richness, as measured by  $M_{\text{HI}}/L_{\text{B}}$ , with FIR luminosity.

It is not obvious that all of the HI that we detect is actually in the polar-ring galaxies themselves. The 21’ beam of the GB 140’ covers a linear diameter of 300 kpc at a distance of 50 Mpc, which is large enough to include close companion galaxies; we list nearby companions in the notes. For ten galaxies in our sample, radio synthesis maps are available from which the mass of gas in the polar ring can be estimated;

in seven of these, this quantity is more than 30% below our measured flux. For five of those seven galaxies, one or more gas-rich companions were detected in synthesis maps, close enough to contribute to the measured Green Bank flux; another has a close neighbor at unknown redshift. Thus the masses that we quote here are only upper limits, and the HI mass in the polar-ring galaxies themselves may be only half or a third as much. Even so, these are gas-rich galaxies, in gas-rich environments.

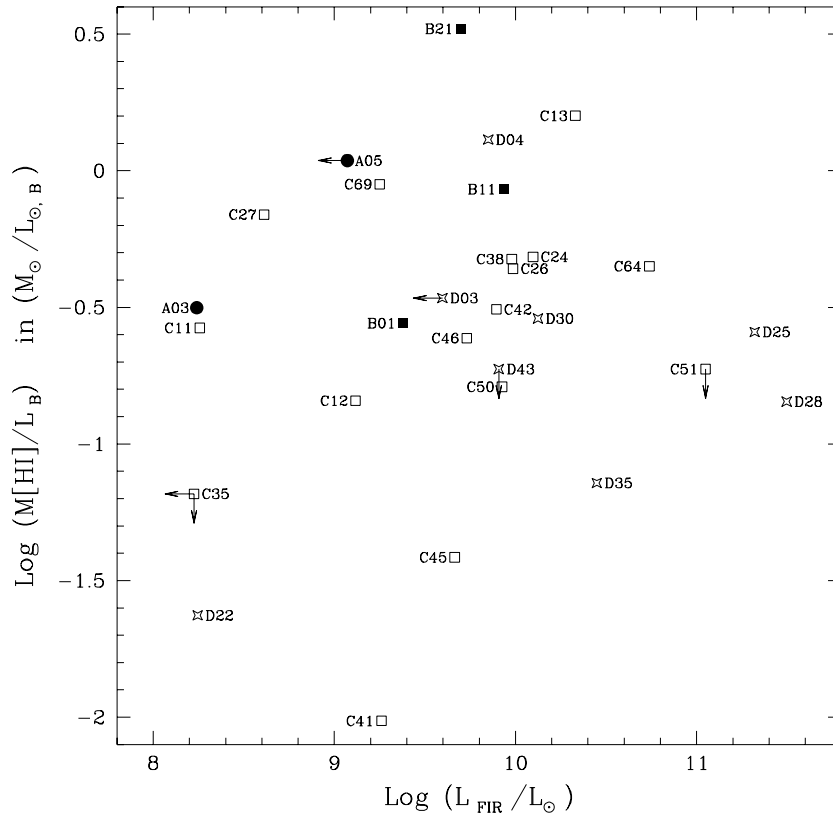


**Fig. 6** The gas-richness,  $M_{\text{HI}}/L_{\text{B}}$ , as a function of far-infrared luminosity for the GB 140' sample; no trend is apparent.

Polar rings are thought to represent captured material, but it is not clear what kind of accretion process would lead to their formation. Capture of gas from a passing spiral seems unlikely, since our observed masses are comparable to the *entire* HI content of a large spiral. The suggestion has been made that the rings represent the remains of a gas-rich dwarf irregular galaxy, which has been captured and torn apart by differential rotation. However, the distribution of HI masses in dwarf irregulars peaks around  $5 \times 10^8 M_{\odot}$  (Matthews, Gallagher & Littleton 1993), a factor of ten below what we find for our polar ring sample. Further, our computed ratios of HI-mass-to-light include the central galaxy, which contributes most of the light but (on the basis

of synthesis maps), almost none of the gas. Thus the accreted object must have been unusually gas-rich, but with an optical luminosity that is small even compared to the relatively dim central galaxies of polar rings. Yet another possibility is that the rings result from the delayed infall of primordial or intragroup gas. Further synthesis observations would establish whether diffuse group gas has contributed substantially to our measured fluxes, since extended emission would be resolved out in those maps. One might question whether such an ordered structure as a polar ring can form out of intragroup gas; but the giant ring in Leo (Schneider *et al.* 1989), a 200 kpc diameter structure containing at least  $10^9 M_{\odot}$  of HI that appears to be in coherent rotation, may be a larger-scale example of such a phenomenon.

## Acknowledgements

It is with pleasure that we thank the telescope operators and other NRAO staff, especially Ron Maddalena, for their high-quality and cheerful support during the observing session. The Green Bank site director G. Seielstad kindly accommodated a delay in the observing run. We are grateful to Michael Strauss and John Huchra for assisting us in our search for optical redshifts, to Marion Schmitz for tracking down the source of a few anomalies in NED, to Frank Briggs for re-reducing VLA archival data of NGC 4650A, and to Harley Thronson and Rick Pogge for several lively e-mail exchanges. This research has made use of the NASA/IPAC Extragalactic Database

(NED). Most of this work was done while OGR was an ESA staff member at STScI. Work by PDS was supported in part by the National Science Foundation (AST 92-15485) and the J. Seward Johnson Charitable Trust. LSS was partially supported by NSF grant AST 90-20650, and thanks the Institute for Advanced Study for hospitality.



## References

- Appleton, P.N. & Struck-Marcell, C. 1987, ApJ, 312, 566
- Balkowski, C., Chamaraux, P., and Weliachew, L. 1978, AA, 69, 263
- Binney, J.J., & Tremaine, S. 1987, *Galactic Dynamics*, (Princeton University Press: Princeton)
- Bland, J., Taylor, K. & Atherton, P. 1987, MNRAS, 228, 595
- Bothun G.D., Mould, J.R., Wirth, A. & Caldwell, N. 1985, AJ, 90, 697
- Bothun, G.D., Lonsdale, C.J. & Rice, W. 1989, ApJ, 341, 129
- Bushouse, H.A., Lamb, S.A. & Werner, M.W. 1988, ApJ, 335, 74
- de Vaucouleurs, G., de Vaucouleurs, A., Corwin, H.G. Jr., Buta, R.J., Paturel, G. & Fouqué, P. 1991, *Third Reference Catalogue of Bright Galaxies*, Univ. of Texas Press, Austin (RC3)
- Eskridge, P.B. & Pogge, R.W. 1991, AJ, 101, 2056
- Gallagher, J.S., Knapp, G.R. & Faber, S.M. 1981, AJ, 86, 1781.
- Giovanelli, R. & Haynes, M.P. 1988, in *Galactic and Extragalactic Radio Astronomy*, 2nd edition, eds. G.L. Verschuur & K.I. Kellerman (Springer: New York), p522
- Graham, J. A. 1979, ApJ, 232, 60
- Hibbard, J.E., Guhathakurta, P., van Gorkom, J.H. & Schweizer F. 1993, submitted to AJ
- Huchra J.P., Geller, M.J., Clemens, C.M., Tokarz, S.P. & Michel, A. 1992, Bull. C.D.S., 41, 31 (Strasbourg) (ZCAT)
- Huchtmeier, W.K., & Richter, O.-G. 1989, *A General Catalog of HI Observations of Galaxies*, Springer-Verlag, New York.
- Jarvis, B.J. 1987, in *Structure and Dynamics of Elliptical Galaxies*, IAU Symposium 127 (Reidel: Dordrecht), p411
- Lauberts, A. 1982, *The ESO-Uppsala Survey of the ESO(B) Atlas*, (ESO: Garching) (ESO)
- Lauberts, A., & Valentijn, E.A. 1989, *The Surface Photometry Catalogue of the ESO-Uppsala Galaxies*, (ESO: Garching) (LV)
- Lonsdale, C.J., Helou, G., Good, J.C., Rice, W. & Fullmer, L. 1989, *Catalogued Galaxies and Quasars in the IRAS Survey*, 2nd version (JPL: Pasadena)
- Mahon, M. E. 1992, PhD Thesis, U. of Florida, Gainesville.
- Matthews, L.D., Gallagher, J.S. & Littleton, J.E. 1993 in *Massive Stars and Their Lives in the Interstellar Medium*, eds. J.P. Cassinelli & E.B. Churchwell (ASP: San Francisco), p501
- Mirabel, I.F. & Sanders, D.B. 1988, ApJ, 335, 104
- Nicholson, R. A., Bland-Hawthorne, J., & Taylor, K. 1992, ApJ, 387, 503

- Nilson, P. 1973, *Uppsala General Catalogue of Galaxies*, Nova Acta Regiae Societatis Scientiarum Upsaliensis, Ser. V:A. Vol. 1 (UGC)
- Rubin, V.C. 1987 in *Dark Matter in the Universe*, IAU Symposium No. 117, eds. J. Kormendy and G. Knapp (Reidel, Dordrecht)
- Sackett, P.D. 1991, in *Warped Disks and Inclined Rings around Galaxies*, eds. S. Casertano, P.D. Sackett & F.H. Briggs (Cambridge University Press: Cambridge), p73
- Sackett, P.D., & Sparke, L.S. 1990, ApJ, 361, 408 (SS)
- Sandage, A. & Tammann, G.A. 1987, *A Revised Shapley-Ames Catalog of Bright Galaxies*, Carnegie Institution of Washington, Publication 635, Second Edition (RSA)
- Schechter, P.L., Sancisi, R., van Woerden, H., & Lynds, C.R. 1984, MNRAS, 208, 111
- Schneider, S., *et al.* 1989, AJ, 97, 666
- Schweizer, F. 1982, ApJ, 252, 455
- Schweizer, F., Whitmore, B.C., & Rubin, V.C. 1983, AJ, 88, 909 (SWR)
- Seitzer P, & Schweizer, F. 1990, in *Dynamics and Interactions of Galaxies*, ed R. Wielen (Springer: Heidelberg), p270
- Shane, W.W. 1980, AA, 82, 314
- Sparke, L.S. 1986, MNRAS, 219, 657
- Sulentic, J.W. & Tifft, W.G. 1973, *The Revised New General Catalog of Nonstellar Astronomical Objects*, (U of Arizona Press: Tucson) (RNGC)
- Thronson, H.A., Bally, J. & Hacking, P. 1989, AJ, 97, 363
- Tully, R.B. 1988, *Catalog of Nearby Bright Galaxies*, (Cambridge University Press) (NBG)
- van Driel, W. & van Woerden, H. 1991, AA, 243, 71
- van Gorkom, J.H., Schechter, P.L., & Kristian, J. 1987, ApJ, 314, 457
- van Gorkom, J.H., van der Hulst, J. M., Haschick, A.D. & Tubbs, A.D., 1990, AJ, 99, 1781
- Wardle, M. & Knapp, G.R. 1986, AJ, 91, 23
- Whitmore B.C. & Bell M. 1988, ApJ, 324, 741
- Whitmore, B.C., McElroy, D., & Schweizer, F. 1987, ApJ, 314, 439 (WMS)
- Whitmore, B.C., Lucas, R.A., McElroy, D.B., Steiman-Cameron, T.Y., Sackett, P.D., & Olling, R.P. 1990, AJ, 100, 1489 (PRC)

## Appendix: Notes on Individual Galaxies

**A-1 = A0136-0801** Our linewidth of  $408 \text{ km s}^{-1}$  is only slightly larger than the  $342 \text{ km s}^{-1}$  measured at the VLA (van Gorkom *et al.* 1987), yet we detected  $5.1 \times 10^9 M_{\odot}$  of HI with the  $20'$ -beam (FWHM) of the Green Bank 140-ft (GB 140'), while the VLA only sees  $1.5 \times 10^9 M_{\odot}$ . NED lists no companions within  $10'$ ; of the two companions within  $20'$ , NGC 636 is outside the velocity range at  $1847 \text{ km s}^{-1}$ , and MCG-01-05-012 is a 15th magnitude galaxy of unknown redshift. The similarity of the linewidths suggests that most of the measured HI mass is associated with the polar-ring system.

**A-2 = ESO 415-G26** We see almost twice as much gas ( $5.4 \times 10^9 M_{\odot}$ ) with a linewidth that is more than  $100 \text{ km s}^{-1}$  larger than indicated by previous VLA observations (van Gorkom *et al.* 1987). The VLA measured  $3.2 \times 10^9 M_{\odot}$  of HI, but missed flux at high relative velocities, especially on the blueward side on the line, due to interference (J. van Gorkom, private communication); this may be responsible for the ‘butterfly contours’ in the total HI map, the smaller linewidth, and higher systemic velocity of the VLA observations. NED reports no companions within  $10'$  and only one galaxy within  $20'$ : RC3 022508–315509, with no listed magnitude but a radial velocity ( $4530 \text{ km s}^{-1}$ ) that places it within the linewidth of ESO 415-G26. It is thus unclear whether all of the HI detected at the GB 140' is associated with the polar-ring system.

**A-3 = NGC 2685** The HI map made at Westerbork by Shane (1980) shows two dynamical systems in HI, one associated with inner optical ‘helix’ that crosses the main optical disk perpendicularly, the other at large radius at a position angle close to that of the central galaxy. His estimate of the total HI mass is  $1.2 \times 10^9 M_{\odot}$ , of which one-quarter is in the central polar ring; our Green Bank observations find a mass of  $1.4 \times 10^9 M_{\odot}$  with nearly the same linewidth of about  $300 \text{ km s}^{-1}$ . New VLA data (Mahon 1992) for this galaxy show  $1.6 \times 10^9 M_{\odot}$  with about the same linewidth. One small, 16th magnitude galaxy lies within  $10'$  of NGC 2685 and two more faint, small galaxies are within  $20'$ . We identify the negative feature at  $1288 \text{ km s}^{-1}$  in the subtracted spectrum of NGC 2685 as an OFF-beam detection of UGC 4549.

**A-5 = NGC 4650A** The GB 140' sees  $6.7 \times 10^9 M_{\odot}$ , 50% more flux than the VLA ( $4.6 \times 10^9 M_{\odot}$ ; van Gorkom *et al.* 1987); the linewidths are quite similar. A preliminary reduction of the VLA archival data (F. Briggs, private communication) shows that the nearby spiral companion, NGC 4650, has a significant amount of HI flux. NGC 4650 is  $5'$  away from NGC 4650A, well inside the GB 140' beam, and has a radial velocity of  $2953 \text{ km s}^{-1}$ , *i.e.*, it is within  $100 \text{ km s}^{-1}$  of NGC 4650A. There are two other companions within  $10'$  and another two within  $20'$  with similar redshifts; this galaxy is in a fairly dense environment.

- A-6 = UGC 9796 = II Zw 73** The GB 140' sees  $2.1 \times 10^{10} M_{\odot}$  of gas, nearly five times as much as the Westerbork synthesis observations reported by Schechter *et al.* (1984) for the polar ring alone; the linewidths are quite similar, but our profile is very asymmetric and is not double-horned. Seven companion galaxies were also detected in the Westerbork map; five of these lie within the GB 140' beam, including the near neighbor MCG +07-31-049 which is separated by 1.5' and  $20 \text{ km s}^{-1}$  from UGC 9796. The companions are partly responsible for the high gas-to-galaxy-light ratio of  $M_{\text{HI}}/L_{\text{B}} = 6.2$  of this system. The total HI mass integrated from the Westerbork map within 12' is  $1.6 \times 10^{10} M_{\odot}$  (R. Sancisi, private communication), close to our result. Although no IRAS flux has been reported for UGC 9796,  $60\mu$  flux has been reported for its companion, MCG +07-31-049.
- B-1 = IC 51 = Arp 230** The coordinates for this shell galaxy are listed incorrectly in the PRC; correct coordinates are given in Table 1. The GB 140' detected  $1.6 \times 10^9 M_{\odot}$  of HI. NED lists no optical companions within 30'.
- B-11 = UGC 5600** This galaxy shows optical emission in a large, diffuse face-on outer ring as well as in the inner, narrow, and apparently edge-on ring that is perpendicular to the position angle of the central object. The total HI mass measured by the GB 140' is  $4.5 \times 10^9 M_{\odot}$ . UGC 5600 is paired with its disturbed companion UGC 5609, which is located at very nearly the same radial velocity ( $2729 \text{ km s}^{-1}$ ) and 2' to the south. NED reports five other galaxies of unknown redshifts within 20'; all but one are faint.
- B-12 = ESO 503-G17** Despite the large distance of this galaxy, its very suggestive morphology warranted inclusion in our sample. Together with its optical redshift, non-detection with the GB 140' implies a weak upper limit of  $M_{\text{HI}} = 2.3 \times 10^{10}$ . No companions listed by NED within 30'.
- B-16 = NGC 5122** An unreliable optical redshift caused us to miss this galaxy in our GB 140' run. The spectrum at the coordinates of NGC 5122, but at a higher, incorrect redshift, is shown in Fig. 1; it appears that there is significant flux at  $4800 \text{ km s}^{-1}$ . Subsequent observations at the VLA (Cox *et al.*, 1994, in preparation) has revealed that about  $5 \times 10^8 M_{\odot}$  of gas is associated with the ring of NGC 5122 itself, and an equal amount is in a companion (MCG-02-34-045) 10' and about  $100 \text{ km s}^{-1}$  away. NED lists no other companions within 20'. The VLA map, along with optical long-slit spectroscopy of the central body (Jarvis and Sackett, unpublished), confirms this galaxy as a polar ring.
- B-17 = UGC 9562 = II Zw 71** We measure a total HI mass of  $9.7 \times 10^8 M_{\odot}$ . A previous synthesis observation at Westerbork (Balkowski *et al.* 1978) indicated a combined HI mass of  $1.1 \times 10^9 M_{\odot}$  for II Zw 71, its companion galaxy II Zw 70 (UGC 9660) which is 4' away, and an intergalactic HI cloud between them.

Their HI map indicates that about  $6.3 \times 10^8 M_{\odot}$  of this gas is associated with the ring of II Zw 71. This is consistent with an Arecibo single-dish observation (*cf.*, Huchtmeier & Richter 1989) which gives a total flux that is two-thirds of that seen with the GB 140', within a beam approximately 3' across.

- B-21 = ESO 603-G21** We measure an HI mass of  $6.4 \times 10^9 M_{\odot}$ . The galaxy has a prominent dust lane that warps across the ring. NED lists only one companion within 20', the peculiar spiral ESO 603-G20, which is 5' away with a redshift ( $3171 \text{ km s}^{-1}$ ) close to that of the polar-ring galaxy. It is likely that this companion contributes part of the flux measured by the GB 140', which may explain the enormously high gas-to-light ratio of  $M_{\text{HI}}/L_{\text{B}} = 3.3$ .
- B-23 = A 2330-3751** Since no redshift is available, the GB 140' observations place an upper limit of about  $2.2 \text{ Jy} \cdot \text{km s}^{-1}$  on the total flux in the 21cm line in the search band ( $1000\text{-}8000 \text{ km s}^{-1}$ ), but do not constrain the total HI mass. This galaxy lies 8.5' from the center of the cluster Abell 4015.
- B-27 = ESO 293-IG17 = AM 2353-392** No redshift is available; our non-detection places an upper limit on the total flux in the 21cm line of about  $2.5 \text{ Jy} \cdot \text{km s}^{-1}$  in the search band ( $1000\text{-}8000 \text{ km s}^{-1}$ ). This galaxy is a member of a projected triple on the sky, and NED lists one other optical companion, ESO 293-G15, 4.4' away.
- C-9 = NGC 442** NED reports no companions within the GB 140' beam that are at a redshift consistent with this marginal detection of  $2.1 \times 10^9 M_{\odot}$  of HI.
- C-11 = NGC 625 = ESO 297-G5** This nearby galaxy is unambiguously detected with the GB 140' with  $1.8 \times 10^8 M_{\odot}$  of HI in a spectrum that also includes HI emission from the Galaxy near zero velocity. There are two galaxies about 11' away: MS 0132.5-4151 has a much higher redshift ( $z = 0.172$ ), while ESO 297-G010 has a blue magnitude of 15.2 and an unknown redshift.
- C-12 = UGC 1198 = VII Zw 3** An extremely marginal detection of  $1.4 \times 10^8 M_{\odot}$  is deduced from the sharp peak at  $1100 \text{ km s}^{-1}$ . A NED search shows no nearby companion.
- C-13 = NGC 660 = UGC 1201** This nearby starburst galaxy contains optically-emitting gas mixed with dust in a warped ring that is highly inclined to the central body. The strong double-horned profile seen with the GB 140' contains  $8.5 \times 10^9 M_{\odot}$  of HI. The nearby UGC 1211 is 16' away with a radial velocity that is  $1600 \text{ km s}^{-1}$  higher than that of NGC 660; it is not a source of confusion for our observations. Previous Arecibo observations (*cf.*, Huchtmeier & Richter 1989) give a flux integral of  $54 \text{ Jy} \cdot \text{km s}^{-1}$ , about one-third of our flux, but since the optical diameter of this galaxy is about 8', the GB 140' beam is well-matched to the size of the system, whereas the 3' Arecibo beam would

be expected to miss emission. New high-resolution VLA observations (Mahon 1992) show about 80% of the GB 140' flux and a slightly larger linewidth. It is likely that all the HI that we detect is in fact associated with NGC 660, which makes it quite gas-rich, with an  $M_{\text{HI}}/L_{\text{B}} = 1.6$ . In the far-infrared, NGC 660 is one of the more luminous galaxies in our sample.

- C-14 = NGC 979 = ESO 246-G23** The outer optical ring is faint and smooth; it may be a face-on polar ring. The GB 140' measured an HI mass of  $2.4 \times 10^{10} M_{\odot}$ , with a large linewidth of  $678 \text{ km s}^{-1}$ ; the profile is single-peaked rather than double-horned. To our knowledge, this detection provides the only known redshift for this galaxy. NED lists one companion within 20': ESO 246-G22, which is 9' away and has an optical radial velocity of  $5127 \text{ km s}^{-1}$ . This companion may have contributed to the measured flux and large velocity spread of the gas.
- C-18 = ESO 358-G20** The GB 140' detects this small galaxy with  $2.2 \times 10^8 M_{\odot}$  of HI in a very asymmetric profile. The galaxy lies near a faint, distant galaxy cluster, but NED lists no companions of similar redshift within 10', and within the GB 140' beam one, ESO 358-G25, at 13' away and a radial velocity of  $1459 \text{ km s}^{-1}$ , which may be responsible for some of the flux in the asymmetric line.
- C-24 = UGC 4261** The GB 140' sees a large HI mass,  $8 \times 10^9 M_{\odot}$  within a slightly asymmetric, but double-horned profile. NED lists no companions within 10', and only two small galaxies within 20'. This and the profile shape suggest that most of the HI is associated with UGC 4261 itself.
- C-25 = UGC 4323** A total HI mass of  $2.2 \times 10^9 M_{\odot}$  is detected by the GB 140' in an asymmetric profile. Emission in the OFF-beam appears as the 'absorption' feature at  $4785 \text{ km s}^{-1}$  in the subtracted spectrum. NED lists no companions within 10'; the galaxy pair including UGC 4353 is about 15' away with a radial velocity of about  $4300 \text{ km s}^{-1}$ , but the GB 140' sees no significant flux at this velocity. Our radio redshift differs from the optical one by about  $300 \text{ km s}^{-1}$ , though our peak flux is much nearer the optical velocity.
- C-26 = UGC 4332** The GB 140' sees  $5.5 \times 10^9 M_{\odot}$  of HI in a somewhat asymmetric profile. The extensive dust on the NE side of the galaxy may be related to its IRAS flux. This galaxy is in a cluster and has many close neighbors. Since the radial velocities (as reported by NED) of the neighbors within the GB 140' beam are smaller than  $5200 \text{ km s}^{-1}$  or larger than  $6500 \text{ km s}^{-1}$ , most of the flux detected at  $5811 \text{ km s}^{-1}$  is likely to be associated with UGC 4332, despite the fact that the line center differs by about  $300 \text{ km s}^{-1}$  from the optical velocity. An OFF-beam detection can be seen in the spectrum at  $5134 \text{ km s}^{-1}$ .
- C-27 = UGC 4385** Clear detection of  $1.2 \times 10^9 M_{\odot}$  of HI within a double-horned profile. NED lists no optical companions within the GB 140' beam.

- C-29 = NGC 2865** Within a double-horned profile, the GB 140' sees  $7.8 \times 10^8 M_{\odot}$  of HI in this shell galaxy. The  $M_{\text{HI}}/L_{\text{B}}$  ratio of this galaxy is only about 0.04. NED lists no companions within the GB 140' beam.
- C-35 = NGC 3414** Our upper limit of  $5.1 \times 10^8 M_{\odot}$  with GB 140' implies a small gas-to-light ratio of  $M_{\text{HI}}/L_{\text{B}} \leq 0.07$ . This galaxy has unusual isophotes and is considered by Whitmore and Bell (1988) to be a box or X-galaxy; it has three neighbors with separations within 10' and redshifts within  $300 \text{ km s}^{-1}$ .
- C-38 = NGC 3934 = UGC 6841** The GB 140' sees  $3.3 \times 10^9 M_{\odot}$  of HI. The baseline was affected by solar interference. NED lists three other galaxies within 15'; two are small and quite faint, but the third, NGC 3933, is only 3' away with a nearly identical radial velocity, and so may be contributing some of the GB 140' flux.
- C-39 = NGC 4174** The GB 140' sees  $7.7 \times 10^9 M_{\odot}$ . This galaxy is in a tight HI-rich group, Hickson 61; NED lists 3 galaxies within 4', two of which have redshifts similar to NGC 4174, and another two with similar redshifts about 20' away. Thus, some of the HI gas detected by the GB 140', including the apparent emission at about  $3650 \text{ km s}^{-1}$ , is probably associated with the group rather than with the polar ring.
- C-41 = IC 3370** Although generally considered a box-shaped elliptical, there is evidence for cylindrical rotation and X-shaped isophotes (Jarvis 1987, Whitmore & Bell 1988, Seitzer and Schweizer 1990). NED lists one other galaxy within the GB 140' beam and three more just outside it, one of which has a redshift nearly identical to that of IC 3370. Our extremely marginal detection of  $5.1 \times 10^8 M_{\odot}$  of HI is shifted by  $300 \text{ km s}^{-1}$  from the optically-determined redshift of the galaxy. We find  $M_{\text{HI}}/L_{\text{B}} < 0.01$ , which makes this system the most gas-poor galaxy in our sample.
- C-42 = NGC 4672** The GB 140' sees  $2.8 \times 10^9 M_{\odot}$  of HI, with a large velocity width, as would be expected if the gas is associated with the extended edge-on component. NED lists three companions within 10' and a further eight, many of which are dwarf ellipticals, within 20'. Two of these galaxies are spirals with radial velocities at the edge of the observed linewidth, and thus might have contributed to the total HI flux seen by the GB 140'.
- C-44 = NGC 5103 = UGC 8388** We obtain a firm detection of  $M_{\text{HI}} = 5.1 \times 10^8 M_{\odot}$  for this system, which optically resembles the Helix galaxy, NGC 2685. NED lists no companions within 10', and only two optical galaxies within 20', both of which appear too faint and distant to be confused with NGC 5103.
- C-45 = Cen A = NGC 5128** Cen A is well-known for its warped lane of gas and dust, which exhibits complicated dynamics (Graham 1979, Bland *et al.* 1987,

Nicholson *et al.* 1992). The HI spectrum is complicated by strong absorption features associated with the Milky Way and with Cen A itself, seen against its strong central continuum. Accordingly, the total HI mass is highly uncertain at  $7.8 \times 10^8 M_{\odot}$  plus or minus 30%, assuming a distance of 3.3 Mpc. With an optical size of over 25', it is possible that some HI flux may lie outside even the GB 140' beam. VLA mapping by van Gorkom *et al.* (1990) showed  $3.1 \times 10^8 M_{\odot}$  of gas, suggesting that there is diffuse or extended emission that was missing from the synthesis maps. Although owing to its proximity Cen A is bright in the far-infrared, its intrinsic far-infrared luminosity is not remarkable in our sample; furthermore, it is relatively gas-poor.

**C-46 = ESO 576-G69** This galaxy is wrapped by a series of optical arcs and also exhibits a spectacular long tidal tail; the GB 140' gives a  $4\text{-}\sigma$  detection of  $3.7 \times 10^9 M_{\odot}$  in HI at a radial velocity  $400 \text{ km s}^{-1}$  larger than the optical redshift. NED lists three other galaxies of unknown redshifts within 10' of ESO 576-G69, as well as an absorption-line system at  $5400 \text{ km s}^{-1}$  seen against a background QSO that lies to the southeast of the galaxy behind an optical filament. Another four galaxies are listed between 10' and 20', including one ESO 576-G64 with a radial velocity of  $5546 \text{ km s}^{-1}$  that makes it a possible source of confusion for the GB 140'.

**C-48 = ESO 326-IG6** The GB 140' gives only a weak upper limit of  $2.1 \times 10^{10} M_{\odot}$  of HI for this small, relatively distant elliptical with outer shell-like optical debris. NED lists no optical companions with 10', but three galaxies within 20', one of which has a radial velocity of  $9633 \text{ km s}^{-1}$ , placing it just at the edge of our bandwidth.

**C-50 = UGC 10205** In many respects, this galaxy looks like a normal Sa galaxy, but its edge-on absorption 'disk' shows evidence for a brightness bump in the light profile (PRC); deep exposures also indicate diffuse debris and shell structure in the outer regions (Rubin, 1987). The GB 140' sees  $3.9 \times 10^9 M_{\odot}$  of HI, which gives it a gas-to-light  $M_{\text{HI}}/L_{\text{B}} = 0.16$ . NED lists no optical companions within the GB 140' beam.

**C-51 = NGC 6285+6286** There is a clear tidal interaction between this close pair; both galaxies show optical debris that is highly inclined to the their central planes, but the more southerly NGC 6286 is the more obvious polar-ring candidate. We centered our band on the wrong velocity at the GB 140'; the redshift listed in PRC is incorrect. Our bandwidth was large enough, however, to cover the optical velocity range of the pair, which allows us to place an upper limit of  $M_{\text{HI}} = 4.2 \times 10^9 M_{\odot}$  for the system. NED lists one companion with 10', UGC 10641, which was a radial velocity of  $5314 \text{ km s}^{-1}$  and is outside our bandwidth. In addition, NED lists four more galaxies of unknown redshifts



within 20'. The pair is infrared luminous; the FIR emission is believed to be associated with NGC 6286 (M. Schmitz, private communication).

**C-60 = ESO 464-G31** This disturbed system appears to consist of two nearly perpendicular edge-on components, one of which is associated with faint, extended debris. GB 140' sees a large amount of gas,  $9.8 \times 10^9 M_{\odot}$ , with a large linewidth, in this somewhat marginal detection. The automated photometry of the ESO-LV catalog (Lauberts & Valentijn 1989) divided this system into two objects of magnitudes 15.02 and 15.64. We summed these magnitudes to obtain the value given in Table 1 and list the larger of the two diameters, although it is also possible that this system is a superposition of two interacting galaxies on the sky. To our knowledge, this represents the first measured redshift of this system. NED lists no other galaxies within the GB 140' beam.

**C-64 = ESO 343-IG13** The X-shaped optical emission in this galaxy, with streamers connecting pairs of legs of the X, is believed to represent the superposition of two interacting galaxies on the sky. The GB 140' detects  $6.2 \times 10^9 M_{\odot}$  of HI in a double-horned profile. The system is one of the more far-infrared luminous galaxies in our sample. NED lists one other galaxy within 10' and another within 20'; both are about 16th magnitude with no listed redshift.

**C-69 = NGC 7468=UGC 12329** The GB 140' makes a strong detection of  $3.6 \times 10^9 M_{\odot}$  of HI in this system. NED lists no other companions within 20', so this system appears to be quite gas-rich, with an  $M_{\text{HI}}/L_{\text{B}} = 0.98$ .

**D-02 = NGC 235** This galaxy, which is sometimes listed as having multiple components, is a member of an interacting pair; optical debris connects it to its southern partner, NGC 232, located about 2' away at a nearly identical redshift. (In both the ESO-LV catalog and NED, two separate components, NGC 235A and NGC 235B, are listed with a separation substantially less than the optical diameter of the galaxy. Checking coordinates against an optical photograph confirms that the companion seen in the PRC is NGC 232.) NED lists two other galaxies with unknown redshifts within the GB 140' beam. The total HI mass for the system reported by the GB 140' is  $5.5 \times 10^9 M_{\odot}$ , some of which may be associated with the neighboring galaxies. Although no far-infrared flux is reported for NGC 235 by NED, the companion NGC 232 is associated with IRAS flux.

**D-03 = ESO 474-IG28** The detection by the GB 140' of  $4.9 \times 10^9 M_{\odot}$  of HI is marginal. NED lists no companions within 10', but three within 20': two with discrepant redshifts, and one with unknown redshift. The OFF-beam detection at  $3059 \text{ km s}^{-1}$  can be seen as the negative feature in the subtracted spectrum.

**D-04 = ESO 296-G11** This system, also called the 'Boomerang,' is thought to be a chance superposition of two galaxies on the sky; unlike some of the other

objects in our sample, there is no evidence for optical tails connecting the two crossed components. The ZCAT and RC3 catalogs give optical redshifts of  $5052 \text{ km s}^{-1}$  and  $5572 \text{ km s}^{-1}$  respectively for this system; interestingly, we appear to have detected emission at both  $5162 \text{ km s}^{-1}$  and  $5593 \text{ km s}^{-1}$ , with respective gas masses of  $1.5 \times 10^{10} M_{\odot}$  in a broad, asymmetric profile and  $1.8 \times 10^9 M_{\odot}$  in a marginal detection the magnitude of which is influenced by the choice of baseline. NED lists no other optical companions within  $10'$ , and two galaxies within  $20'$ : one very faint galaxy of unknown redshift, and another galaxy with a brightness comparable to ESO 296-G11 with a radial velocity of  $6576 \text{ km s}^{-1}$ . In order to compute the luminosities and their ratios given in two separate lines in Table 3 for this system, we have assumed as limiting cases that all of the blue and far-infrared flux is associated entirely with one of the two HI redshifts systems. At least one of these systems must be quite gas-rich.

**D-22 = NGC 4643** A very faint, disk-like feature is aligned with the major axis and extending to three times the optical diameter of this otherwise normal-looking barred spiral (*cf.*, PRC). The GB  $140'$  detection is at a radial velocity more than  $300 \text{ km s}^{-1}$  lower than the quoted optical velocity. Since NED lists no optical companions within  $10'$ , and one small galaxy of unknown redshift within  $20'$ , most of the  $1.1 \times 10^8 M_{\odot}$  of HI seen by the GB  $140'$  is probably associated with this system. Nevertheless, its gas-to-light ratio of about  $M_{\text{HI}}/L_{\text{B}} = 0.02$  is smaller than average for an SB0/a (Giovanelli & Haynes 1988).

**D-25 = UGC 8387 = IC 883** The disturbed morphology of this galaxy includes two linear, one-sided and almost perpendicular optical features protruding from center. The galaxy is quite infrared-luminous. The GB  $140'$  finds  $6.1 \times 10^9 M_{\odot}$  of neutral hydrogen. NED lists one faint galaxy of unknown redshift within  $10'$ , and one faint galaxy and a faint galaxy cluster within  $20'$ . Thus, most of the gas is probably associated with UGC 8387 itself. Mirabel and Sanders (1988) observed this galaxy with the smaller beam of the Arecibo radio telescope and found a broad, triple-peaked absorption feature against the continuum. This complicates the interpretation of our emission feature; the system may contain more gas than we have estimated.

**D-28 = NGC 6240 = UGC 10592** This superluminous IRAS galaxy is a merger product: short exposures reveal many crossed optical loops and deeper exposures show an extensive set of shells. The GB  $140'$  reports a gas mass of  $8.2 \times 10^9 M_{\odot}$  within an irregular profile of large linewidth (about  $600 \text{ km s}^{-1}$ ). Since this galaxy is a radio source, it is possible that our emission spectrum is being influenced by absorption against the continuum. NED lists no optical companions within  $10'$ , and only one fairly faint galaxy within the GB  $140'$  beam.

**D-30 = ESO 341-IG4** The GB  $140'$  reports a firm detection of  $1.4 \times 10^{10} M_{\odot}$  of HI in this system, which according to NED has no neighbors within  $10'$ . One

galaxy and a galaxy cluster, both at higher redshift, do lie within the GB 140' beam.

**D-35 = NGC 7252** This, the famous ‘Atoms for Peace’ galaxy studied by Schweizer (1982), is the most optically-luminous and one of the more infrared-luminous galaxies in our sample. The galaxy is an obvious merger product, as evidenced by the remarkable optical loops and tidal tails surrounding it. The GB 140' detects  $4.5 \times 10^9 M_{\odot}$  of HI, which given the large blue luminosity of this galaxy, makes it gas-poor compared to others in our sample. The linewidth of  $200 \text{ km s}^{-1}$  seems surprisingly low given the disturbed optical morphology of the system. VLA observations (Hibbard *et al.* 1993) show  $3.6 \times 10^9 M_{\odot}$  of HI in NGC 7252, tails and all, and a further  $1.4 \times 10^9 M_{\odot}$  in an uncatalogued companion, A2218-248, about  $12'$  and  $50 \text{ km s}^{-1}$  away. The sum of these two fluxes is within 15% of our measured value.

**D-43 = ESO 510-G13** This boxy system has a very thin optical disk and an associated dust lane along its major axis. Probably for this reason, the automated photometry routines of ESO-LV catalog have broken the system into two fainter ‘galaxies,’ one associated with the flat disk and one with the boxy feature. We have therefore used the magnitude and diameter quoted from RC3 for inclusion in Table 1. The GB 140' reports an upper limit for the HI mass of this system of  $3.3 \times 10^9 M_{\odot}$ . No other galaxies are reported by NED to be within the GB 140' beam.



**Table 1.** Basic Optical and HI Data for the Green Bank Sample of Polar-Ring Galaxies

PRC No. (1)	Name (2)	R.A.	Dec.	$v_{\text{opt}}$		$B_{\text{T}}$		Log		$v_{\text{HI}}$ [km s <sup>-1</sup> ] (11)	$\int S * dv$	
		(1950.0) (3)	(4)	[km s <sup>-1</sup> ] (5)	(6)	[ <sup>m</sup> ] (7)	(8)	$D_{25}/0.1'$ (9)	(10)		[Jy · km s <sup>-1</sup> ] (12)	(13)
A-01	A0136-0801	01 36 25.4	-08 01 24	5528	S	15.82	P	1.0	T	5521	3.82	1.2
A-02	ESO 415-G26	02 26 11.5	-32 06 14	4560	W	14.7	R	1.12	R	4572	6.22	1.8
A-03	NGC 2685	08 51 41.2	+58 55 30	869	R	12.12	R	1.65	R	875	34.2	4.0
	NGC 2685 OFF <sup>1</sup>	08 41 11	+58 55 30	(1288)	R	13.98	R			1288	6.87	0.87
A-05	NGC 4650A	12 42 04.8	-40 26 35	2904	W	14.27	P	1.20	R	2909	23.2	2.4
A-06	UGC 9796	15 14 00	+43 22 00	5606	Z	16.04	P	1.14	R	5423	16.4	1.7
B-01	IC 51 <sup>2</sup>	00 43 53	-13 42 58	1758	H	13.	N	1.13	R	1709	11.5	1.2
B-11	UGC 5600	10 19 16.6	+78 52 51	2823	R	14.19	R	1.15	R	2769	12.0	1.3
B-12	ESO 503-G17	11 24 24	-27 25 48	10313	J	16.54	P	0.85	LV	9800-11900	< 5.48	
B-16	NGC 5122 <sup>3</sup>	13 21 36	-10 23 39	2861	J					4804	3.96	1.2
B-17	UGC 9562	14 49 13.1	+35 44 53	1236	R	14.41	R	0.98	R	1239	13.6	1.6
B-21	ESO 603-G21	22 48 41	-20 30 42	3150	P	15.5	LV	0.92	LV	3180	14.3	1.3
B-23	A2330-3751	23 30 01	-37 51 09					1.1	T	1000-8000	< 2.18	
B-27	ESO 293-IG17 <sup>4</sup>	23 53 53	-39 26 42			16.17	LV	0.86	LV	1000-8000	< 2.45	
C-09	NGC 442	01 12 05.1	-01 17 05	5620	R	14.45	R	0.99	R	5629	1.53	0.9
C-11	NGC 625	01 32 55.0	-41 41 18	383	R	11.71	R	1.76	R	394	37.4	4.3
C-12	UGC 1198	01 40 58	+85 00 38	1207	H	14.8	R	1.00	R	1149	1.64	1.3
C-13	NGC 660	01 40 20.8	+13 23 20	823	R	12.02	R	1.92	R	848	187.8	50
C-14	NGC 979	02 29 46.2	-44 44 38			13.78	R	1.07	R	4775	26.2	7.4
C-18	ESO 358-G20	03 32 53	-32 47 42	1853	R	14.54	R	1.08	R	1799	1.75	0.6
C-24	UGC 4261	08 07 40.3	+36 58 40	6419	H	14.78	R	0.96	R	6410	4.62	0.8
C-25	UGC 4323	08 15 36.6	+67 08 22	3981	H	14.08	R	1.20	R	3686	3.56	1.0
	UGC 4323 OFF									4785	1.35	0.3
C-26	UGC 4332	08 16 43.1	+21 16 22	5505	R	14.82	R	1.12	R	5811	3.96	1.4
	UGC 4332 OFF	08 27 13	+21 16 22							5134	1.67	0.5
C-27	UGC 4385	08 21 04.2	+14 54 56	1969	Z	14.51	R	0.94	R	1954	7.93	0.9
C-29	NGC 2865	09 21 14.6	-22 56 47	2611	R	12.57	R	1.39	R	2772	2.95	0.40
C-35	NGC 3414	10 48 31.8	+28 14 28	1434	R	11.96	R	1.55	R	400-2300	< 7.13	
C-38	NGC 3934	11 49 38	+17 07 44	3626	R	14.5	R	1.03	R	3793	5.71	0.7
C-39	NGC 4174	12 09 54.9	+29 25 42	3980	R	14.31	R	0.92	R	3811	12.9	4.0
C-41	IC 3370	12 24 58	-39 03 41	2930	R	11.99	R	1.46	R	3219	1.42	0.7
C-42	NGC 4672	12 43 30	-41 26 00	3389	R	14.09	R	1.31	R	3242	7.67	2.5

Table 1. (continued)

PRC No. (1)	Name (2)	R.A. Dec. (1950.0)		$v_{\text{opt}}$ [km s <sup>-1</sup> ]		$B_{\text{T}}$ [ <sup>m</sup> ]		Log D <sub>25</sub> /0.1'		$v_{\text{HI}}$ [km s <sup>-1</sup> ] (11)	$\int S * dv$ [Jy · km s <sup>-1</sup> ] (12) (13)	
		(3)	(4)	(5)	(6)	(7)	(8)	(9)	(10)			
C-44	NGC 5103	13 18 17.6	+43 20 45	1283	R	13.6	R	1.16	R	1289	6.76	0.9
C-45	NGC 5128	13 22 31.8	-42 45 30	538	R	7.84	R	2.41	R	524	300	100
C-46	ESO 576-G69	13 27 22	-20 40 36	5336	H	14.6	LV	0.95	LV	5759	2.91	0.9
C-48	ESO 326-IG6	14 08 04.7	-39 52 15	8584	R	15.	E	1.23	R	7600-9600	< 7.13	
C-50	UGC 10205	16 04 40.6	+30 14 06	6605	R	14.4	R	1.16	R	6773	1.96	0.5
C-51	NGC 6285+6286 <sup>5</sup> NGC 6285/6 OFF	16 57 47	+58 59 47	5595	R	14.06	R	1.12	R	5350-7350 5639	< 3.00 2.47	0.5 0.5
C-60	ESO 464-G31 <sup>6</sup>	21 15 25	-27 33 35			14.5	LV	1.07	LV	6529	5.42	1.9
C-64	ESO 343-IG13 <sup>7</sup>	21 33 05	-38 46 06	5685	R	14.55	R	1.17	R	5716	4.55	1.5
C-69	NGC 7468	23 00 30.3	+16 20 04	5822 2123	R	14.16	R	0.96	R	2072	16.1	1.2
D-02	NGC 235	00 40 24	-23 48 55	6664	R	14.08	R	1.12	R	6710	2.84	1.1
D-03	ESO 474-IG28 ESO 474-IG28 OFF	00 45 06	-23 04 24	6780	H	14.91	LV	0.87	LV	6610 3059	2.62 5.31	1.0 1.6
D-04	ESO 296-G11 <sup>8</sup>	01 17 43	-41 29 55	5052 5572	Z R	14.5	R	1.01	R	5162 5593	14.0 1.38	2.6 0.9
D-22	NGC 4643 NGC 4643 OFF	12 40 46.9 12 30 22	+02 15 06 +02 15 00	1399	R	11.72	R	1.49	R	1053 2199	3.20 1.67	0.8 0.7
D-25	UGC 8387	13 18 17	+34 24 03	6892	R	14.4	R	1.19	R	7024	2.95	1.0
D-28	NGC 6240	16 50 27.7	+02 29 00	7351	R	13.8	R	1.33	R	7197	3.78	1.4
D-30	ESO 341-IG4	20 37 59	-38 22 20	5973	R	13.38	R	1.28	R	6055	9.05	1.3
D-35	NGC 7252	22 17 57.7	-24 55 51	4760	R	12.59	R	1.29	R	4752	4.58	0.56
D-43	ESO 510-G13	13 52 14	-26 32 18	3559	R	13.35	R	1.29	R	2600-4500	< 7.13	

The letters listed in Columns 6, 8 and 10 of Table 1 refer to the following sources for optical redshifts, blue magnitudes and  $m_{\text{HI}}$ : W = WMS; R = RC3; Z = ZCAT, 1992; H = J. Huchra, private communication 1993; J = Jarvis & Sackett, unpublished; Revised NGC; LV = ESO-LV Catalog, Lauberts & Valentijn 1989; E = ESO Catalog, Lauberts, 1982; and T = This work; from photographs published in the PRC.

<sup>1</sup> We identify the signal in the off-beam of NGC 2685 as UGC 4549. Independent *radio* observations give the same velocity; no

<sup>2</sup> The coordinates quoted in the PRC for IC 51 are incorrect; we give the correct coordinates here.

<sup>3</sup> Due to an unreliable redshift, our Green Bank bandpass missed this galaxy, but did make an unrelated detection at about 48

<sup>4</sup> Flux blending from neighbors make the total B magnitude reported from the ESO-LV catalog for this system somewhat uncer

<sup>5</sup> NGC 6285/6286 is an interacting pair; NGC 6286 is the polar-ring candidate. NGC 6285 has a heliocentric velocity of 5696 k

<sup>6</sup> Automated photometry broke this system into two objects; see notes for further explanation.

<sup>7</sup> ESO 343-IG13 is an interacting pair of galaxies that are superimposed on the sky.

<sup>8</sup> ESO 296-G11 is a superposition of two galaxies. We have found two optical redshifts in the literature; apparently our survey



**Table 2.** Basic Infrared Data for the Green Bank Sample of Polar-Ring Galaxies

PRC No. (1)	Galaxy Name (2)	IRAS Reference (3)	Flux Densities [Jy]				Flux Qualities				Log( $F_{\text{FIR}}$ ) [W m <sup>-2</sup> ] (12)	(13)
			12 $\mu$ (4)	25 $\mu$ (5)	60 $\mu$ (6)	100 $\mu$ (7)	12 $\mu$ (8)	25 $\mu$ (9)	60 $\mu$ (10)	100 $\mu$ (11)		
A-01 A-02 A-03 A-05 A-06	A 0136-0801 ESO 415-G26 NGC 2685 NGC 4650A UGC 9796 <sup>1</sup>	FSC2 FSC2	0.09842 <0.09979	< 0.09758 < 0.1515	0.3156 0.3662	1.694 < 1.503	3 1	1 1	3 3	2 1	-13.50 < -13.51	
B-01 B-11 B-12  B-17 B-21 B-23 B-27	IC 51 UGC 5600 ESO 503-G17  UGC 9562 ESO 603-G21 A 2330-3751 <sup>2</sup> ESO 293-IG17	FSC2 FSC2  FSC2	0.1557 0.1544  0.1574	0.2004 0.6052  < 0.1530	2.214 3.464  1.454	4.691 4.961  2.889	2 3  2	2 3  1	3 3  3	2 2  2	-12.88 -12.76  -13.08	- -  -
C-09 C-11 C-12 C-13  C-14 C-18 C-24 C-25  C-26 C-27 C-29 C-35  C-38 C-39 C-41 C-42	NGC 442 <sup>2</sup> NGC 625 UGC 1198 NGC 660  NGC 979 ESO 358-G20 UGC 4261 UGC 4323 <sup>2</sup>  UGC 4332 UGC 4385 NGC 2865 NGC 3414  NGC 3934 NGC 4174 <sup>3</sup> IC 3370 NGC 4672	FSC2 FSC2 FSC2 SCANS  FSC2  FSC2 FSC2 FSC2 FSC2  FSC2 FSC2 FSC2 FSC2	0.1997 0.06611 2.421 2.88	0.9473 0.4148 7.526 7.71	5.094 2.53 65.54 69.92	9.079 2.958 102.04 101.5	3 2 2 R	3 3 3 MR	3 3 3 MR	2 2 2 UR	-12.55 -12.92 -11.47 -11.45	- - - -
			<0.1015	0.1553	1.143	1.345	1	2	3	2	-13.27	
			<0.1995	0.2315	0.8074	2.089	1	2	3	2	-13.28	
			<0.07956	< 0.2213	0.3124	0.8685	1	1	3	2	-13.68	
			<0.1161	< 0.1556	0.1907	< 0.9129	1	1	3	1	< -13.75	
			0.1242	< 0.1553	2.22	4.277	2	1	3	2	-12.90	
			<0.1244	< 0.1010	0.5559	1.595	1	1	3	2	-13.42	
			0.1452	0.2263	2.391	6.641	3	3	3	2	-12.79	-



**Table 2.** (continued)

PRC No. (1)	Galaxy Name (2)	IRAS Reference (3)	Flux Densities [Jy]				Flux Qualities				Log( $F_{\text{FIR}}$ ) [ $\text{W m}^{-2}$ ] (12)
			$12\mu$ (4)	$25\mu$ (5)	$60\mu$ (6)	$100\mu$ (7)	$12\mu$ (8)	$25\mu$ (9)	$60\mu$ (10)	$100\mu$ (11)	
C-44	NGC 5103										
C-45	NGC 5128	FSC2	13.26	17.26	162.2	313.8	3	3	2	2	-11.03
		MAP	23.03	30.74	217.6	501.2					-10.87
C-46	ESO 576-G69	FSC2	<0.1192	0.1568	0.3609	1.581	1	2	3	2	-13.50
C-48	ESO 326-IG6										
C-50	UGC 10205	FSC2	<0.08905	< 0.08411	0.3939	1.538	1	1	3	2	-13.49
C-51	NGC 6285+6286 <sup>4</sup>	FSC2	0.3305	0.4941	7.8778	22.60	3	3	3	2	-12.27
		SCANS	0.50	0.64	9.87	22.01	R	R	MR	UR	-12.22
C-60	ESO 464-G31										
C-64	ESO 343-IG13	FSC2	0.2795	0.8804	5.855	8.906	3	3	3	2	-12.52
C-69	NGC 7468	FSC2	<0.09844	< 0.1439	1.250	1.489	1	1	3	2	-13.23
D-02	NGC 235 <sup>5</sup>										
D-03	ESO 474-IG28	FSC2	<0.09424	< 0.08158	0.2417	< 0.6439	1	1	3	1	< -13.80
D-04	ESO 296-G11 <sup>6</sup>	FSC2	<0.08711	0.09338	0.8823	1.578	1	2	3	2	-13.31
D-22	NGC 4643	FSC2	<0.09545	< 0.1077	0.5018	1.858	1	1	3	2	-13.40
D-25	UGC 8387	FSC2	0.2628	1.362	15.44	25.18	3	2	2	2	-12.09
		SCANS	0.26	1.37	33.69	24.9	UR	UR	UR	UR	-12.12
D-28	NGC 6240	FSC2	0.5578	3.417	22.68	7.78	3	3	3	2	-11.96
D-30	ESO 341-IG4	FSC2	0.1189	0.2719	1.308	1.858	2	3	3	2	-13.18
D-35	NGC 7252	FSC2	0.2398	0.4322	3.975	7.017	3	3	3	2	-12.66
D-43	ESO 510-G13	FSC2	<0.1598	< 0.2401	1.682	6.063	1	1	3	2	-12.88

The flux qualities listed in columns 8-11 are taken from Version 2 of the IRAS Faint Source Catalog (FSC2), where 1 is low and 3 is high quality. For systems in which integrated fluxes from scans or IR maps were available, the columns 8-11 indicate whether the source was detected with IRAS: R = resolved; MR = marginally resolved; UR = unresolved. Beam sizes are  $0.77'$ ,  $0.78'$ ,  $1.44'$ , and  $2.94'$  for the  $12\mu$ ,  $25\mu$ ,  $60\mu$ , and  $100\mu$  bands, respectively.

<sup>1</sup> Although no flux is reported in any IRAS band for UGC 9796, 0.1866 Jy in the  $60\mu$ -band was detected from its companion NGC 4174.

<sup>2</sup> Version 1 of the IRAS Faint Source Catalog reported marginal detection in one band only; FSC2 does not report a detection.

<sup>3</sup> No IRAS flux is reported for NGC 4174, but significant flux in all for IRAS bands are reported for one member of its triplet.

<sup>4</sup> NGC 6285/6286 is an interacting pair; NGC 6286 is the polar-ring candidate and the apparent source of the IRAS flux (M. Schramm et al. 2003).

<sup>5</sup> No IRAS flux is reported for NGC 235, but significant flux in all for IRAS bands are reported for its close companion, NGC 235A.

<sup>6</sup> ESO 296-G11 is a superposition of two galaxies; it is uncertain which one is the source of the IRAS flux.

**Table 3.** Derived Quantities for the Green Bank Sample of Polar-Ring Galaxies

PRC No. (1)	Galaxy Name (2)	Radio Telescope (3)	Distance [Mpc] (4)	$M_{\text{HI}}$ [ $10^9 M_{\odot}$ ] (5)	$L_{\text{B}}$ [ $10^9 L_{\odot, \text{B}}$ ] (6)	$L_{\text{FIR}}$ [ $10^9 L_{\odot}$ ] (7)	$M_{\text{HI}}/L_{\text{B}}$ [ $M_{\odot}/L_{\odot, \text{B}}$ ] (8)	$L_{\text{FIR}}/L_{\text{B}}$ (9)	$M_{\text{HI}}$ [ $M_{\odot}$ ] (10)
A-01	A 0136-0801 <sup>1</sup>	GB140 VLA D	75.1 75.1	5.07 1.48	4.52 4.53		1.12 0.326		
A-02	ESO 415-G26 <sup>1</sup>	GB140 VLA CD/BC	60.5 60.9	5.37 3.20	7.72 7.83		0.695 0.409		
A-03	NGC 2685 <sup>2</sup>	GB140 WBORK VLA	13.3 13.2 13.4	1.42 1.21 1.63	4.52 4.47 4.56	0.174 0.173 0.176	0.315 0.271 0.357	0.296	
A-05	NGC 4650A <sup>1</sup>	GB140 VLA CD/BC	35.0 35.0	6.68 4.62	6.13 6.13	<1.18 <1.18	1.09 0.753	<1.48	>
A-06	UGC 9796 <sup>3</sup>	GB140 WBORK	73.8 73.6	21.0 4.59	3.37 3.35		6.24 1.37		>
B-01	IC 51	GB140	24.2	1.59	5.75	2.40	0.277	3.20	
B-11	UGC 5600	GB140	39.6	4.45	5.19	8.59	0.857	12.7	
B-12	ESO 503-G17	GB140	134	<23.1	8.49		<2.72		
B-17	UGC 9562	GB140	17.4	0.968	0.808		1.20		
B-21	ESO 603-G21	GB140	43.7	6.42	1.94	4.99	3.31	19.7	
B-23	A 2330-3751	GB140							
B-27	ESO 293-IG17	GB140					<1.09		
C-09	NGC 442	GB140	77.1	2.14	17.8		0.121		
C-11	NGC 625	GB140	4.5	0.182	0.685	0.181	0.266	2.03	
C-12	UGC 1198	GB140	18.7	0.135	0.937	1.31	0.144	10.7	
C-13	NGC 660	GB140	13.9	8.52	5.35	21.4	1.59	29.6	
C-14	NGC 979	GB140	62.4	24.1	18.7		1.29		
C-18	ESO 358-G20	GB140	22.9	0.217	1.25		0.174		
C-24	UGC 4261	GB140	85.9	8.02	16.6	12.5	0.484	5.77	
C-25	UGC 4323	GB140	51.3	2.21	10.7		0.207		

**Table 3.** (continued)

PRC No. (1)	Galaxy Name (2)	Radio Telescope (3)	Distance [Mpc] (4)	$M_{\text{HI}}$ [ $10^9 M_{\odot}$ ] (5)	$L_{\text{B}}$ [ $10^9 L_{\odot, \text{B}}$ ] (6)	$L_{\text{FIR}}$ [ $10^9 L_{\odot}$ ] (7)	$M_{\text{HI}}/L_{\text{B}}$ [ $M_{\odot}/L_{\odot, \text{B}}$ ] (8)	$L_{\text{FIR}}/L_{\text{B}}$ (9)	$M_{\text{HI}}/$ [ $M_{\odot}/$ ] (10)
C-26	UGC 4332	GB140	76.8	5.50	12.5	9.69	0.438	5.93	0
C-27	UGC 4385	GB140	24.9	1.16	1.68	0.410	0.691	1.87	2
C-29	NGC 2865	GB140	33.5	0.781	21.4		0.0365		
C-35	NGC 3414	GB140	17.4	<0.509	7.76	<0.168	<0.0657	<0.166	<8
C-38	NGC 3934	GB140	49.2	3.25	6.85	9.53	0.475	10.7	0
C-39	NGC 4174	GB140	50.3	7.72	7.57		1.02		
C-41	IC 3370	GB140	39.1	0.511	52.5	1.82	0.0097	0.267	0
C-42	NGC 4672	GB140	39.4	2.81	9.02	7.84	0.311	6.67	0
C-44	NGC 5103	GB140	17.9	0.512	1.81		0.282		
C-45	NGC 5128	GB140	3.3	0.781	20.3	4.62	0.0385	1.75	0
C-46	ESO 576-G69	GB140	73.8	3.73	15.3	5.39	0.244	2.71	0
C-48	ESO 326-IG6	GB140	111	<20.7	21.1		<0.985		
C-50	UGC 10205	GB140	91.5	3.87	23.9	8.43	0.162	2.70	0
C-51	NGC 6285+6286	GB140	77.4	<4.24	22.6	112	<0.188	38.1	<0
C-60	ESO 464-G31	GB140	87.6	9.81	24.1		0.408		
C-64	ESO 343-IG13	GB140	76.1	6.20	13.9	54.8	0.447	30.3	0
C-69	NGC 7468	GB140	31.0	3.63	4.07	1.78	0.892	3.36	2
D-02	NGC 235	GB140	90.2	5.45	31.2		0.174		
D-03	ESO 474-IG28	GB140	88.9	4.88	14.3	<3.95	0.342	<2.12	>1
D-04	ESO 296-G11 <sup>4</sup>	GB140	68.2	15.3	11.8	7.07	1.30	4.60	2
	(superposition)	GB140	73.5	1.76	13.7	8.21	0.128	4.60	0
D-22	NGC 4643	GB140	11.9	0.107	4.53	0.176	0.0236	0.299	0
D-25	UGC 8387	GB140	93.8	6.11	23.8	209	0.257	67.3	0
D-28	NGC 6240	GB140	96.1	8.23	57.7	314	0.143	41.7	0
D-30	ESO 341-IG4	GB140	80.4	13.8	49.5	13.3	0.288	2.07	1
D-35	NGC 7252	GB140	64.3	4.46	62.0	28.1	0.0720	3.48	0
D-43	ESO 510-G13	GB140	44.4	<3.31	17.7	8.09	<0.188	3.51	<0

<sup>1</sup> Results quoted from VLA observations are those of van Gorkom, Schechter, and Kristian (1987).

<sup>2</sup> Westerbork observations of NGC 2685 are from Shane (1980); VLA observations are those of Mahon (1992).

<sup>3</sup> Westerbork observations of UGC 9796 are those of Schechter, *et al.* (1984).

<sup>4</sup> ESO 296-G11 is a superposition of two galaxies; we detect HI at two different redshifts. The quantities  $L_{\text{B}}$  and  $L_{\text{FIR}}$  shown in the two rows for this galaxy have been computed as if all of flux originated from one of the two redshifts.